Gadolinium oxysulfide nanoprobes with both persistent luminescent and magnetic properties for multimodal imaging

C. Rosticher, Bruno Viana, M.-A. Fortin, J. Lagueux, L. Faucher, Corinne Chanéac

ARTICLE

Gadolinium oxysulfide nanoprobes with both persistent luminescent and magnetic properties for multimodal imaging

Received 00th January 20xx,
Accepted 00th January 20xx

DOI: 10.1039/x0xx00000x

www.rsc.org/

C. Rosticher[a], B. Viana[b*], M.-A. Fortin[c,d,e], J. Lagueux[e] and L. Faucher[c,d,e], C. Chanéac[a*]

Persistent luminescence and magnetic properties of Gd_2O_2S: Eu^{3+}, Ti^{4+}, Mg^{2+} nanoparticles have been studied to attest the relevance of such nanoparticles as nanoprobes for multimodal imaging. The development of new imaging tools is required to improve the quality of medical images and then to diagnose some disorders as quickly as possible in order to ensure more effective treatment. Multimodal imaging agents here developed combine the high resolution abilities of Magnetic Resonance Imaging (MRI) with another more sensitive technique, like optical imaging, leading significant possibilities for early detection of diseases and a better understanding of pathologies. Recently, inorganic persistent luminescent nanoparticles (i-PLNPs) have been reported as suitable probes for *in vivo* imaging that meet the difficulties due to the biological environment. The i-PLNPs are first excited by a UV light for a few minutes outside the animal before injection and emit in the border of the red/NIR window for hours after the injection. In this paper, we explore a new chemical composition of host lattice doped with transition metal and lanthanide ions for persistent luminescence that contains a paramagnetic centre conferring additional magnetic properties for a use in MRI, and that can be obtained at the nanoscale. Thus, advanced Gd_2O_2S nanoparticles exhibiting both persistent luminescence and paramagnetic properties have been synthesized and fully characterized. Their luminescent properties were determined as well as their magnetic properties. One compound sample with composition Gd_2O_2S: Eu^{3+} (5%), Ti^{4+} (1%), Mg^{2+} (8%) presents both optical and magnetic properties suitable for a bimodal imaging probe. Indeed, it shows an afterglow in the red range at 620 nm and a relaxivity corresponding to r_2 / r_1 ratio of 1.28.

Introduction

In the field of medical imaging, the development of new imaging tools is a challenging task to obtain more reliable and early diagnosis. There are many categories of *in vivo* imaging techniques, using different electromagnetic radiations, and each one shows some advantages and limits. Combining imaging techniques gives the opportunity to improve the diagnoses by generating more accurate images [1-6]. MRI is a non-invasive and widely used imaging technique that produces excellent soft tissue diagnosis and spatial resolution. However, for an imaging modality to be optimum, a high sensitivity is also needed, and MRI shows poor sensitivity. In contrast, optical imaging presents an exquisite sensitivity but has limited spatial resolution. The most attractive combinations are then made of a highly resolved modality (MRI) and a complementary highly sensitive one (optical imaging or PET). Therefore, multimodal imaging probes are also required to combine the advantages of several techniques and overcome their limits. The development of such sophisticated imaging agents has greatly increased the ability to diagnose diseases and provide image guided therapy or track efficacy of treatments [7-9].

In literature, MRI contrast agents have been already coupled with fluorescent molecules to create multimodal imaging probes [10-13] but these fluorescent agents are not very stable and the optical imaging by fluorescence of biological tissue is hampered by absorbance of incident and emitted light [14] and tissue's autofluorescence [15]. These two phenomena reduce the detection limits and restrict the depth of photons penetration into tissues [15]. Using persistent luminescent probes open the path to enhanced signal-to-noise ratio [16,17] and the possible imaging of deep organs by removing absorption and autofluorescence phenomena [16,17]. Indeed new long luminescent nanoparticles that emit in the red-near infrared range inside the biological tissue wavelength therapeutic window (600-1350 nm) were recently proposed for *in vivo* imaging [16-23] as these i-PLNPs avoid tissue's absorption and prevent tissue's autofluorescence since they are excited before the injection or by long wavelengths. Silicates nanoparticles, including doped silicates ($CaMgSi_2O_6$ doped

[a] *Sorbonne Universités, UPMC Univ Paris 06, CNRS, Collège de France, Laboratoire de Chimie de la Matière Condensée de Paris, 11 place Marcelin Berthelot, 75005 Paris, France. * corinne.chaneac@upmc.fr*
[b] *PSL Research University, Chimie ParisTech - CNRS, Institut de Recherche de Chimie Paris, 11 rue Pierre et Marie Curie, 75005 Paris, France. * bruno.viana@chimie-paristech.fr*
[c] *Centre de recherche du centre hospitalier universitaire de Québec (CR-CHUQ), axe Médecine régénératrice, Québec QC, G1L 3L5, Canada.*
[d] *Centre de recherche sur les matériaux avancés (CERMA), Université Laval, Québec QC, G1V 0A6, Canada.*
[e] *Centre de recherche du Centre hospitalier universitaire de Québec (CR-CHUQ), axe Oncologie, Québec QC, G1L 3L5, Canada.*
DOI: 10.1039/x0xx00000x

Eu^{2+}, Mn^{2+}, Dy^{3+} or Pr^{3+}), gallates ($ZnGa_2O_4$: Cr^{3+}) and others were reported [17-29]. In order to obtain a bimodal agent for magnetic resonance and optical imaging, gadolinium oxysulfide nanoparticles, Gd_2O_2S, doped Eu^{3+}, Ti^{4+} and Mg^{2+} were developed within this work. Indeed, gadolinium compounds are well-known to improve the T_1-weighted contrast in the same way as T_2 Fe_2O_3 based contrast agents [30-32]. Both gadolinium compounds and iron oxide achieve highly sensitive MRI and can be used selectively as white and black dual label to detect two cell types simultaneously at any tissue depth [33]. In addition, gadolinium oxysulfide is also well known to be a good matrix for rare earth (RE) emission. Eu^{3+} doped Gd_2O_2S nanoparticles exhibit a strong emission band centred at 624 nm after excitation at 363 nm usual for *in vitro* fluorescence microscopy, whereas Gd_2O_2S: Er,Yb compounds are applicable for deep *in vivo* fluorescence imaging since both excitation (980 nm) and emission (670 nm) are located inside the "transparency window" of biological tissues [34]. Persistent luminescence properties require codoping of the matrix. Zhang *et al.* proved that Gd_2O_2S codoping Er^{3+}, Ti^{4+} in bulk materials also allows to obtain a long luminescence time compared to Er^{3+} single doping [35]. The first long afterglow oxysulfide was produced with the matrix Y_2O_2S doped Eu^{3+}, Ti^{4+}, Mg^{2+}, whose luminescence time in the red could reach 3 hours [36]. At present, no persistent luminescent nanoprobes based on Gd_2O_2S matrix have been reported in the literature. However, several rare earth (RE = Eu, Sm, Dy, Ho, Er and Tm) cations were proposed in Gd_2O_2S solid state compounds with Ti^{4+}, Mg^{2+} as codoping to be relevant to obtain afterglow [37,38]. Here the focus will be on the nanoparticles preparation and, as *in vivo* imaging application required red/ near infrared persistent luminescence detected by the silicon detector, we focused our attention on Gd_2O_2S: Eu^{3+}, Ti^{4+}, Mg^{2+} compounds, trivalent europium being the recombination center with intensive emission in the red.

Despite these effective MRI contrast enhancements, the use of gadolinium compounds as MRI agent is still controversial and less popular than iron oxides, generally known to be biocompatible, because of their potential toxicity [39]. It has been shown that the release of Gd^{3+} ions inside organs causes toxic effect such as nephrogenic systemic fibrosis (NSF) [40]. Nevertheless, several studies have shown that the control of the size of gadolinium oxide nanoparticles can significantly reduce the risk of release of Gd^{3+} ions [41] as well as the encapsulation of the magnetic core by a biocompatible shell [42]. For example, using small size (< 5 nm), the fast excretion of nanoparticles *via* a renal clearance minimizes its toxicity. Such "safe by design" approach is especially required for the development of gadolinium based probes for imaging. In the case of gadolinium oxysulfide, toxic issue is reduced compared to oxide due to the lower solubility [34] opening new opportunities for such compounds.

In this paper, the development of persistent luminescent and paramagnetic Gd_2O_2S nanoparticles as multimodal imaging agents used in MRI and optical imaging is described. Imaging abilities are explored alone and successively. In order to obtain nanoprobes, a hydrothermal synthesis using a chemical sulfurated agent was used, therefore allowing a fast and secure synthesis. Indeed, most of the Gd_2O_2S nanoparticles syntheses using hydrothermal route require an annealing step under inert (Ar or N_2)/CS_2/sulfur/carbon atmosphere at high temperature for the sulfuration of oxide matrix [43, 44]. Using a sulfured flow to anneal the materials is quite dangerous and difficult to use safely in a laboratory. Therefore, we propose to synthesize Gd_2O_2S nanoparticles using a three-steps hydrothermal route. In the second step, thioacetamide, a chemical sulfured agent is added to the solution that decomposes during heating following the reaction: $(CH_3)CS(NH_2) + 2\ H_2O \rightarrow CH_3COO^- + NH_4^+ + H_2S$. This way, the synthesis is safer and faster. These nanosensors can act as multimodal agents for possible *in vivo* optical imaging and MRI imaging.

Experimental

Synthesis

In a typical synthesis, 0.9 mM of $Gd(NO_3)_3.6H_2O$ were dissolved in 16 ml of deionized water to form a clear solution with precursors $EuCl_3.6H_2O$, $Mg(NO_3)_2.6H_2O$ and $TiCl_4$. The pH of the solution was adjusted to 8 by adding NaOH solution under vigorous stirring. The mixture was stirred and heated at 70°C for 2 hours. A white precipitate is obtained, corresponding mainly to $Gd(OH)_3$ phase. An excess of thioacetamide was added to the mixture and then transferred to a Teflon lined stainless steel autoclave and heated at 200°C for 2 hours. A yellowish precipitate was collected, purified, and dried in air at ambient temperature. At this moment, the sulfuration process is not subsequent and an annealing step is needed. Therefore, in order to convert all the product to the formation of Eu^{3+}, Ti^{4+}, Mg^{2+} - doped gadolinium oxysulfide, the collected powder is heated at 700°C for 2h under inert (Ar) atmosphere.
In the aim of improving the persistent luminescence, we vary the doping ratio of the samples: Eu^{3+} (2.5% or 5%), Ti^{4+} (1 to 4%) and Mg^{2+} (2 to 8 %).

Materials and methods

As obtained solids were analyzed by powder X-ray diffraction (PW-XRD) using a Bruker D8 Advance diffractometer using Cu-Kα radiation (λ = 1.5418Å) at 45 kV and 40 mA, 0.0046°2θ step size and 0.5s step time over a range of 10 to 80° - 2θ. Fourier-Transform Infra-Red (FT-IR) spectroscopy has been operated on a Perkin Elmer 400 spectrometer using the universal ATR sampling holder. Transmission Electron Microscopy (TEM) images were acquired with a FEI Tecnai 120 Twin microscope operating at 120 kV and equipped with a high resolution Gatan Orius CCD 4 k 64 k numeric camera. Excitation and emission spectra were measured with a Varian Cary Eclipse Fluorescence spectrophotometer at room temperature. Persistent luminescence spectra were recorded after 2 minutes irradiation with UV light (365 nm-6 W) and the resulting signal was collected *via* an optical fiber by Roper

Scientific Pixis 100 CCD camera cooled at -68°C coupled with an Acton SpectraPro 2150i spectrometer for spectral analysis. Thermoluminescence (TL) measurements were performed with a Ris∅ TL/OSL reader model TL/OSL-DA-15A/B with an EMI 9635QA PM tube. TL glow curves were measured at heating rate of 5°C/s. TL emission spectra were measured using an UV-VIS spectrometer (Avantes, PC2000). For the emission spectra measurements the samples were irradiated with 340 nm UV light for 2 minutes.

The relaxometric properties of the suspensions of magnetic nanoparticles were studied by relaxometric and MRI analysis. For this, the dried particles (30 mg) were dispersed in 10 mL of nanopure water (18.2 MΩ·cm), followed by vortexing (30 sec) and sonication (30 min). To eliminate agglomerates, all suspensions were centrifuged (3000 g, 15 min). From this suspension, 1.5 mL of sample was extracted for relaxometric experiments (T_1 and T_2 measurements) and MRI analysis.

Relaxometric analysis: 400 μL dilutions (100, 90, 80, 70, 50 % v/v) of the previous suspension in pure water were distributed in 6.0 mm NMR tubes. Longitudinal and transversal relaxation times (T_1 and T_2) were measured with a dedicated TD-NMR relaxometer (Bruker Minispec 60 MHz, 37°C). The relaxation rates ($1/T_1$ and $1/T_2$) were then plotted against Gd concentration values, and relaxivities (r_1 and r_2) were calculated from the slope of the graphs. To quantify the concentration of Gd in each suspension, the 100% and 50 % v/v samples were digested in nitric acid and hydrogen peroxide, and analyzed in ICP-MS.

MRI analysis: Dilutions of the samples were imaged with a 1 T small-animal MRI system (M2M, Aspect Imaging, Netanya, Israel) using T_1-weighted spin-echo sequences (repetition time: 400 ms; echo time: 10.8 ms; dwell time: 16; matrix: 200 × 200; slice thickness: 1.9 mm; interslice: 0.1 mm; field of view: 70 mm; 3 excitations; 25°C). The suspensions were stable in time according to MRI measurements (for a few days), even after centrifugation.

Results and discussion

Structure and morphology of Gd_2O_2S: Eu^{3+}, Ti^{4+}, Mg^{2+} nanostructures

Main characterizations reported in this paper correspond to Gd_2O_2S doped with Eu^{3+} (5%), Ti^{4+} (1%), Mg^{2+} (2%). FTIR spectrum shows an important absorption around 3500 and 1500 cm^{-1} which corresponds to the presence of hydroxyl groups (Fig. 1a). Gd_2O_2S: Eu^{3+}, Ti^{4+}, Mg^{2+} products showed pronouncing features in the range 1700–600cm^{-1}. The intense absorption peak at 600 cm^{-1} may be attributed to (Gd/Eu–O) and (Gd–S) groups. Absorption bands at 1400 and 1100 cm^{-1} may indicate the presence of (C–O) and (S–O) modes respectively [43, 44].

The purity and crystallinity of the products were examined using powder XRD. PW-XRD patterns obtained from the Gd_2O_2S: Eu^{3+}, Ti^{4+}, Mg^{2+} products are shown in Fig. 1b. All peaks can be indexed as the pure hexagonal Gd_2O_2S phase and

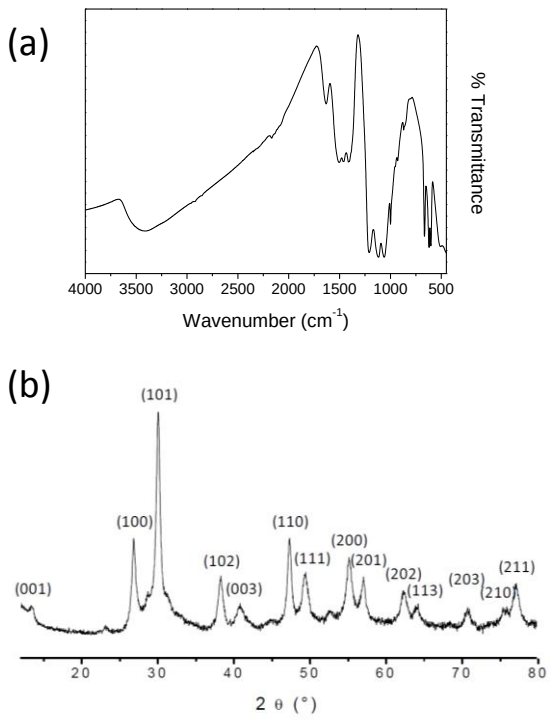

Fig. 1 (a) FTIR spectrum and (b) XRD pattern of Eu^{3+}, Ti^{4+}, Mg^{2+} doped Gd_2O_2S compound after 2h annealing at 700°C under argon.

they are in good agreement with standard Gd_2O_2S data ([P3m1, 164], JCPDS # 27-1422; lattice constant: a=b= 3.784 Å, c= 6.589 Å). Zhang *et al.* showed that the insertion of doping elements such as Eu^{3+}, Ti^{4+} or Er^{3+}, in a gadolinium oxysulfide does not perturb the crystalline structure of the matrix in the long range [35]. Particles size and crystalline structure observed by XRD are not modified by the presence of doping elements in the oxysulfide matrix.

The morphology of Gd_2O_2S: Eu^{3+}, Ti^{4+}, Mg^{2+} nanoparticles greatly depends on the pH during the hydrothermal synthesis [43,44]. At pH=8, most of the obtained nanoparticles exhibit a facetted shape (Fig. 2a) with smaller spherical nanoparticles (Fig. 2.b) with size below 20 nm. Shaped nanoparticles diameter is between 50 and 100 nm. In good agreement with Ref. 44, such morphologies were favoured by the pH= 8 value

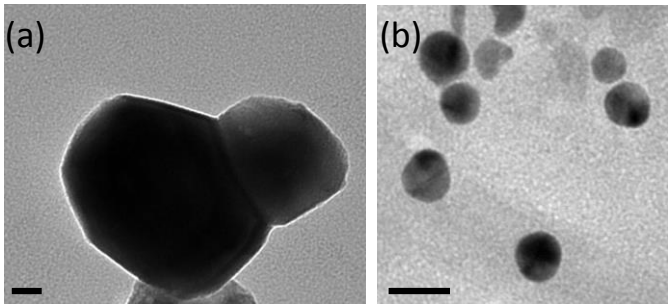

Fig. 2 TEM images of Eu^{3+}, Ti^{4+}, Mg^{2+} doped Gd_2O_2S nanoparticles after 2h annealing at 700°C under argon. Scale bars are 20 nm.

chosen for the synthesis. These morphologies and sizes well below 100 nm are well adapted to *in vivo* application.

The main synthesis step that influences the size of the nanoparticles is the thermal treatment under argon. In order to study the effect of the annealing treatment on the particle size, the heating time and temperature were varied. Compounds obtained after the second step of hydrothermal synthesis were annealed from 700 to 1100°C for 2 or 4 hours. The main objective was to determine the most efficient thermal treatment in terms of crystallinity, purity, size and luminescence. TEM images of the annealed samples are shown in Fig. 3. The particles size increases with the annealing temperature from 50 nm to 100 nm for temperatures comprised between 700 and 1100°C respectively. The sintering becomes more and more important with the increase of annealing time and temperature. Therefore, for a temperature of 1100°C, bigger nanoparticles and many aggregates are obtained because of the sintering effect (Fig. 3e-j). The aggregates are more abundant for thermal treatments of 4 hours. For *in vivo* applications, small nanoparticles are needed and aggregates have to be avoided at the most. Therefore the most efficient annealing treatment for gadolinium oxysulfide in terms of size, crystallinity and dispersity is a treatment at 700°C, for 2h under argon. Spherical and facetted nanoparticles with a diameter ranging between 50-80 nm were then obtained as seen in Fig. 3.

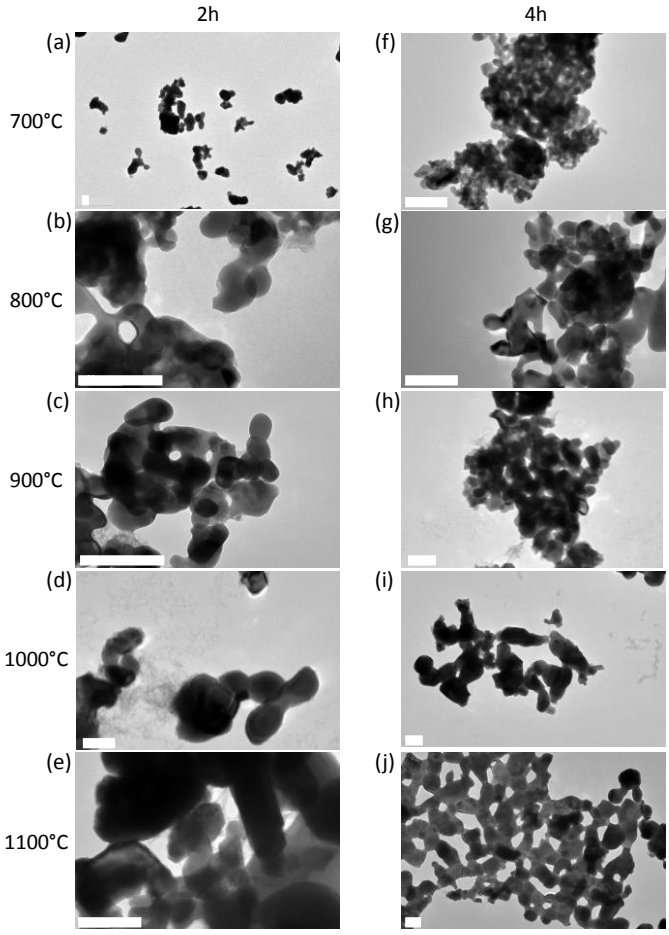

Fig. 3 TEM images of Eu^{3+}, Ti^{4+}, Mg^{2+} doped Gd_2O_2S nanoparticles depending on annealing treatment under argon: (a) 700°C-2h ; (b) 800°C-2h ; (c) 900°C-2h ; (d) 1000°C-2h ; (e) 1100°C-2h ; (f) 700°C-4h ; (g) 800°C-4h ; (h) 900°C-4h ; (i) 1000°C-4h ; (j) 1100°C-4h. All scale bars are 100 nm.

Emission

Fig. 4 represents the emission and excitation spectra of Eu^{3+}, Ti^{4+}, Mg^{2+} doped Gd_2O_2S nanoparticles (annealed at 700°C under argon for 2h) recorded at room temperature after 100 μs delay. The emission spectrum (Fig. 4b) under excitation at 325 nm shows emission bands peaking between 580 nm and 720 nm, attributed to Eu^{3+} emission. The peaks located at 584 nm, 595 nm, 618 nm, and 715 nm correspond to the well known $^5D_0 \rightarrow {}^7F_j$ radiative transitions of Eu^{3+}. Because of the 100us delay, no emission could be observed form the $^5D_1$ or $^5D_2$ levels.

This reveals that Eu^{3+} ions are indeed the luminescent centers in the Eu^{3+}, Ti^{4+}, Mg^{2+} doped Gd_2O_2S compound. The excitation spectrum (Fig. 4a) for an emission at 618 nm consists of two intensive bands peaking at 330 nm and 227-250 nm corresponding to the charge transfer from S^{2-} to Eu^{3+} and to the host Gd_2O_2S absorption respectively [45,46]. In addition the peaks at 395 nm are characteristic of the Eu^{3+} *4f-4f* transitions.

It can be noticed that the excitation spectrum of gadolinium oxysulfides as observed Fig. 4a is closer to the one of oxides reported in the literature than sulfides. This may be linked to the direct environment of cations in oxysulfides composed of 4 oxygen atoms and 3 sulfur atoms with oxygen much closer to gadolinium than sulfur. Then, the energy levels of trivalent rare earth cations in Gd_2O_2S energy diagram as reported in Ref [47] is more similar to oxide host rather than sulfide matrix.

Persistent luminescence properties

Fig. 5 shows the evolution of the persistent luminescence recorded at room temperature depending on Mg^{2+} doping ratio in Gd_2O_2S doped Eu^{3+}, Ti^{4+}, Mg^{2+} after switching off the UV source at room temperature, before and after annealing treatment at 700°C under argon for 2h, and UV excitation (at 340 nm for 2 min). In addition one should indicate that the non-annealed sample shows no persistent luminescence.

The sulfuration step which takes place during the annealing treatment at high temperature is therefore compulsory to allow persistent luminescence. During this thermal treatment, anionic vacancies could be created such as S^{2-} vacancies (see after the TSL glow curves), that can explain the necessity of the thermal treatment as these vacancies have a key role in the persistent luminescence mechanism. After annealing, the persistent luminescence spectra of Gd_2O_2S: Eu^{3+} (5%), Ti^{4+} (1%), Mg^{2+} (x%) exhibit the usual three emission bands at 585 nm, 620 nm and 705 nm which indicate that trivalent europium is the recombination center. These emission bands are attributed to the radiative $^5D_0 \rightarrow {}^7F_j$ transitions of Eu^{3+}. The

most intense centred at 620 nm, corresponds to $^5D_0 \rightarrow {}^7F_2$ transition.

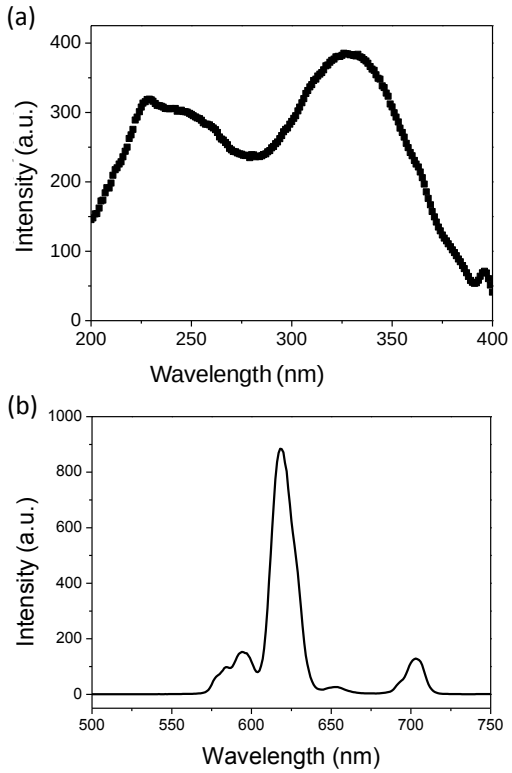

Fig. 4 (a) Excitation of the 618 nm emission and (b) emission spectrum under 325 nm excitation of Gd_2O_2S: Eu5%, Ti1%, Mg8% nanoparticles at room temperature after 100 μs time delay.

Increasing Mg^{2+} doping ratio has an important effect on persistent luminescence in Gd_2O_2S doped Eu^{3+}, Ti^{4+}, Mg^{2+}. Therefore higher is Mg^{2+} doping ratio, more intense is the persistent luminescence in agreement with the stoichiometry of the compounds, divalent magnesium required charge compensation that can be done by sulfur vacancies and increased the TSL signal presented in the following part of the paper. This indicates the major role of the divalent magnesium in the persistent luminescence mechanism, creating intermediate traps levels in the bandgap of the material. Such traps creation, is an important step to enhance the persistent luminescence.

Decay curves were recorded during ~~2 minutes~~ few seconds after switching off the UV excitation (Fig. 5b). Their non-exponential profiles show that several types of traps are present within Gd_2O_2S: Eu^{3+}, Ti^{4+}, Mg^{2+} compounds. Again decrease of persistent luminescence intensity is noted when Mg^{2+} doping ratio decreases. The optimal doping ratio for Gd_2O_2S doped Eu^{3+}, Ti^{4+}, Mg^{2+} compounds was determined to be Eu^{3+} (5%), Ti^{4+} (1%), Mg^{2+} (8%).

The thermoluminescence curve of Gd_2O_2S: Eu^{3+} (5%), Ti^{4+} (1%), Mg^{2+} (8%) is displayed in Fig. 6. The sample was heated up to 400°C prior excitation to empty all the charges traps. Then it was excited under UV light for 2 minutes. The emission spectrum is recorded after switching off the excitation while heating the sample up to 300°C by a 5°C/sec step. This heating step empties the charges traps filled during the excitation step.

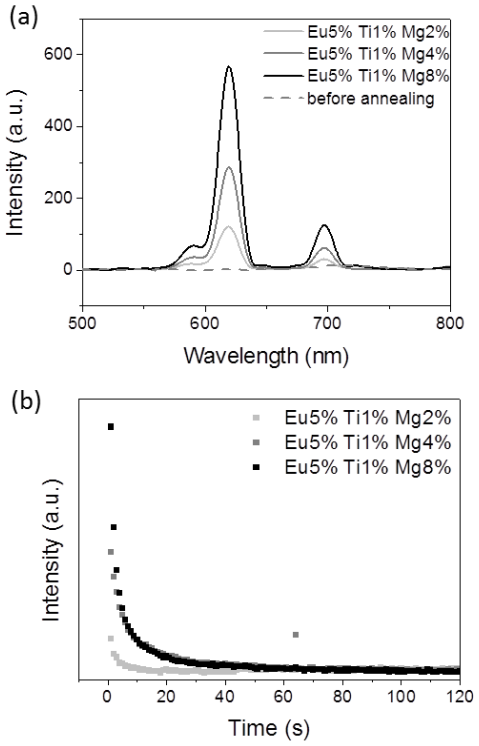

Fig. 5 (a) Persistent luminescence spectra of Gd_2O_2S: Eu5%, Ti1%, Mgx% compounds – λexc = 365 nm – excitation time = 2 min. Spectra recorded few seconds after the end of the excitation. (b) Luminescence decay curves depending on Mg ratio for Gd_2O_2S: Eu5%, Ti1%, Mgx% compounds – λexc = 365 nm – excitation time = 2 min.

One strong peak is observed between 30 and 125°C with a maximum at 55°C.

The trap depth E with respect to the conduction band edge can be roughly estimated by the simple expression $E \approx 0.002T_M$ [48], where T_M is the temperature of the peak maximum. Experimental value of trap depth was found to be 0.65 eV. This value is coherent with literature data [37,38]. This indicates that these shallow traps are at the origin of the persistent luminescence and the shape of the glow curve observed in Fig. 6 also indicates that there are no deeper traps in the sample. In oxysulfide matrix, there are possibly three types of traps-defects: isoelectronic traps due to Eu^{3+}, charges traps resulting of the substitution of nonequivalent ions (Mg^{2+}, Ti^{4+}) and anionic vacancies (such as S^{2-}, and possibly also O^{2-}). Trivalent europium is the recombination center and can also act as electron trap in the Gd_2O_2S matrix ($Eu^{3+} + e^- \Leftrightarrow Eu^{2+*}$). Titanium (IV) could also be an electron trap ($Ti^{4+} + e^- \rightarrow Ti^{3+*}$). The role of the divalent magnesium can be to favour the stoichiometry variation as divalent cation replaces a trivalent one with a charge compensation, which in turns favours anionic vacancies. Furthermore Mg^{2+} doping induces the formation of intermediate energy levels, allowing important

energy storage inside the matrix and thus longer decay [36]. Finally anionic vacancies such as S^{2-}, and possibly also O^{2-} are also well known electron traps [49]. Distances between gadolinium cations and sulfur or oxygen anions in the matrix are d_{Gd-S} = 2.852 Å and d_{Gd-O} = 2.329 Å / 2.399 Å respectively. Thus sulfur vacancies should be easier to form as Gd-S distances are larger in comparison to the Gd-O ones. However, even knowing the role of each ion in the persistent luminescence mechanism, one cannot fully conclude which traps (Eu^{3+}, Ti^{4+} or anionic vacancies S^{2-} and O^{2-}) are responsible for the peak observed in TSL glow curve (Fig. 6) in the Gd_2O_2S: Eu^{3+}, Ti^{4+}, Mg^{2+} compounds.

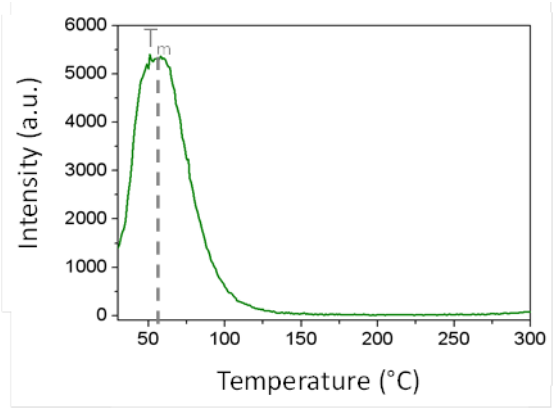

Fig. 6 TSL glow curve of Gd_2O_2S: Eu5%, Ti1%, Mg8% nanoparticles. (rise temperature of 5°C/s)

Relaxometry and magnetic properties (MRI)

Longitudinal and transversal relaxation times (T_1 and T_2) of diluted suspensions of Gd_2O_2S: Eu^{3+} (5%), Ti^{4+} (1%), Mg^{2+} (8%) were measured with a dedicated TD-NMR relaxometer. Then, these suspensions were imaged with a 1T small-animal MRI system. Fig. 7 shows the longitudinal and transversal relaxation curves of diluted suspensions of Gd_2O_2S: Eu^{3+} (5%), Ti^{4+} (1%), Mg^{2+} (8%) recorded at 37°C. *In vitro* results show that doped Gd_2O_2S nanoparticles present a longitudinal relaxivity of 6.7 $mM^{-1}s^{-1}$, which is close to the reported values for Gd_2O_3 nanoparticles of similar size [30-31,50-51]. The relaxometric ratio (r_2/r_1), which indicates the capacity of the contrast agent to provide "positive" contrast in T_1-weighted imaging (close to 1), or "negative" contrast, in T_2-weighted imaging (typically higher than 2), is 1.28. This clearly indicates the capacity of Gd_2O_2S: Eu^{3+} (5%), Ti^{4+} (1%), Mg^{2+} (8%) to provide strong "positive" contrast enhancement in T_1-w. imaging. The strong T_1 effect on signal was confirmed on MRI coronal images (Fig. 7b). The signal from ^1H protons in the vicinity of a "positive" contrast agent is usually greatly enhanced using short echo times and spin echo T_1-weighted sequences (as in Fig. 7b). Although more refined relaxometric characterization would be necessary, and in particular NMRD (nuclear magnetic relaxation dispersion) profiles, to confirm the exact mechanism of relaxivity, it is clear that a strong exchange occurs between H_2O protons and surface paramagnetic ions. As reflected by the moderate T_2 values, the nanoparticles are clearly paramagnetic, without evidence of superparamagnetism that would have lead to much higher r_2 values.

(a)

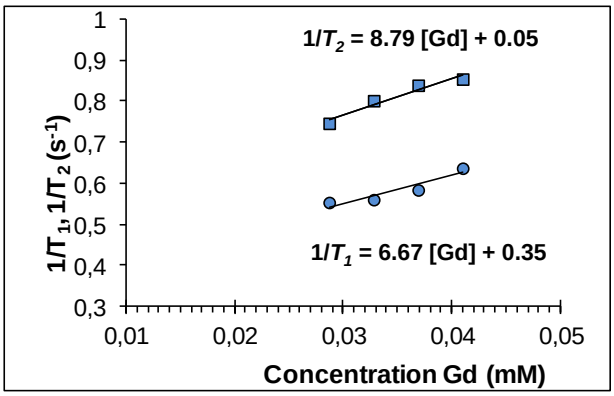

(b)

[Gd] (10^{-4}mM) 0.041 0.037 0.033 0.029

Fig. 7 (a) ^1H relaxation rates measured with Gd_2O_2S: Eu5%, Ti1%, Mg8% aqueous suspensions. (b) Resulting MR-images (1.5 T, 21°C; T_1-weighted fast spin-echo; TR, 400 ms; TE, 10.8 ms).

Conclusions

Gd_2O_2S doped Eu^{3+}, Ti^{4+}, Mg^{2+} nanoparticles were prepared using a three-steps hydrothermal synthesis. Nanoparticles morphology and size were controlled by pH and annealing treatment. In the aim of improving the red-near infrared persistent luminescence at about 620 nm, different doping ratios were studied. We obtained an optimal composition with larger magnesium content: Gd_2O_2S doped Eu^{3+} (5%), Ti^{4+} (1%), Mg^{2+} (8%). In that case persistent luminescence can be observed within several minutes for the first time in the gadolinium oxysulfide nanoparticles. Relaxometric and magnetic resonance imaging properties were investigated, and Gd_2O_2S: Eu^{3+} (5%), Ti^{4+} (1%), Mg^{2+} (8%) showed a high T_1 effect with a relaxation ratio of 1.28. This compound proved to be a promising positive contrast agent. Then Gd_2O_2S doped Eu^{3+} (5%), Ti^{4+} (1%), Mg^{2+} (8%) nanoparticles combine optical imaging agent with persistent luminescence properties and a good MRI contrast agent because of its relaxation properties. *In vivo* study of the bimodal properties will be the next research step for this compound.

Acknowledgements

We thank Patrick Le Griel for his help during TEM experiments and Adrie Bos from Delft University of Technology for TSL experiments. This work was supported by the French Research National Agency (ANR) in the frame of its program in Nanosciences and Nanotechnologies (Natlurim project n°ANR-08-NANO-025).

References

1 T. Skajaa, D. P. Cormode, E. Falk, W. J. M. Mulder, E. Fisher and Z. A. Fayad, *Arterioscler. Thromb, Vasc. Biol.*, 2010, **30**, 169.
2 J. Yang, E. K. Lim, H. J. Lee, J. Park, S. C. Lee, K. Lee, H. G. Yoon, J. S. Suh, Y. M. Huh and S. Haam, *Biomaterials*, 2008, **29**, 2548.
3 W. J. M. Mulder, G. J. Strijkers, G. A. F. van Tilborg, D. P. Cormode, Z. A. Fayad and K. Nicolay, *Acc. Chem. Res.*, 2009, **42**, 904.
4 J. Kim, Y. Piao and T. Hyeon, *Chem. Soc. Rev.*, 2009, **38**, 372.
5 W. J. M. Mulder, D. P. Cormode, S. Hak, M. E. Lobatto, S. Silvera and Z. A. Fayad, *Nat. Clin. Pract. Cardiovasc. Med.*, 2008, **5**, S103.
6 M. M. Hüber, A. B. Staubli, K. Kustedjo, M. H. B. Gray, J. Shih, S. E. Fraser, R. E. Jacobs and T. J. Meade, *Bioconjugate Chem.*, 1998, **9**, 242.
7 K. Y. Choi, G. Liu, S. Lee and X. Chen, *Nanoscale*, 2012, **4**, 330.
8 J. V. Jokerst and S. S. Gambhir, *Acc. Chem. Res.*, 2011, **44**, 1050.
9 T. Maldiney, B. T. Doan, D. Alloyeau, M. Bessodes, D. Scherman and C. Richard, *Adv. Funct. Mater.*, 2015, **25**, 331.
10 B. Brooksby, B. W. Pogue, S. Jiang, H. Dehghani, S. Srinivasan, C. Kogel, T. D. Tosteson, J. Weaver, S. P. Poplack and K. D. Paulsen, *Proc. Natl. Acad. Sci. USA.*, 2006, **103**, 8828.
11 Y. Koyama, V. S. Talanov, M. Bernardo, Y. Hama, C. A. S. Regino, M. W. Brechbiel, P. L. Choyke and H. J. Kobayashi, *Magn. Reson. Imaging*, 2007, **25**, 866.
12 A. Bumb, C. A. Regino, M. R. Perkins, M. Bernardo, M. Ogawa, L. Fugger, P. L. Choyke, P. J. Dobson and M. W. Brechbiel, *Nanotechnology*, 2010, **21**, 175704.
13 W. J. M. Mulder, G. J. Strijkers, R. Koole, C. D. M. Donega, G. Storm, A. W. Griffioen and K. Nicolay, Bimodal Liposomes and Paramagnetic QD-Micelles for Multimodality Molecular Imaging of Tumor Angiogenesis in Nanoparticles in Biomedical Imaging; *Springer: New York*, 2007.
14 W. F. Cheong, S.A. Prahl and A.J. Welch, *IEEE J. Quantum Electron.*, 1990, **26**, 2166.
15 J. V. Frangioni, *Curr. Opin. Chem. Biol.*, 2003, **7**, 626.
16 T. Maldiney, A. Bessière, J. Seguin, E. Teston, S. K. Sharma, B. Viana, A. J. J. Bos, P. Dorenbos, M. Bessodes, D. Gourier, D. Scherman and C. Richard, *Nat. Mater.*, 2014, **13**, 418.
17 Q. Le Masne De Chermont, C. Chanéac, J. Seguin, F. Pellé, S. Maitrejean, J. P. Jolivet, D. Gourier, M. Bessodes and D. Scherman, *Proc. Natl. Acad. Sci. USA*, 2007, **104**, 9266.
18 T. Maldiney, G. Sraiki, B. Viana, D. Gourier, C. Richard, D. Scherman, M. Bessodes, K. Van den Eeckhout, D. Poelman and P. F. Smet, *Opt. Mater. Express*, 2012, **2**, 261.
19 Y. Li, S. Zhou, G. Dong, M. Peng, L. Wondraczek and J. Qiu, *Sci. Rep.*, 2014, **4**, 4059.
20 X. Fu, C. Liu, J. Shi, H. Man, J. Xu and H. Zhang, *Opt. Mater.*, 2014, **36**, 1792.
21 F. Liu, W. Yan, Y.-J. Chuang, Z. Zhen, J. Xie and Z. Pan, *Sci. Rep.*, 2013, **3**, 1554.
22 Z. Li, J. Shi, H. Zhang and M. Sun, *Opt. Express*, 2014, **22**, 10509.
23 B. Viana, S. K. Sharma, D. Gourier, T. Maldiney, E. Teston, D. Scherman and C. Richard, *J. Lumin.*, 2016, 170, 879.
24 A. Lecointre, B. Viana, Q. LeMasne, A. Bessiere, C. Chaneac and D. Gourier, *J. Lumin.*, 2009, **129**, 1527.
25 A. Lecointre, A. Bessiere, B. Viana and D. Gourier, *Radiat. Meas.*, 2010, **45**, 497.
26 T. Maldiney, A. Lecointre, B. Viana, A. Bessiere, M. Bessodes, D. Gourier, C. Richard and D. Scherman, *J. Am. Chem. Soc.*, 2011, **133**, 11810.
27 A. Bessiere, S. K. Sharma, N. Basavaraju, K. Priolkar, L. Binet, B. Viana, A. Bos, T. Maldiney, C. Richard, D. Scherman and D. Gourier, *Chem. Mater.*, 2014, **26** (3), 1365.
28 C. Rosticher, B. Viana, G. Laurent, P. Le Griel, and C. Chanéac, *Eur. J. Inorg. Chem.,* 2015, 3681.
29 C. Rosticher, B. Viana, T. Maldiney, C. Richard and C. Chanéac, *J. Lumin.*, 2016, **170**, 460.
30 L. Faucher, M. Tremblay, J. Lagueux, Y. Gossuin and M. A. Fortin, *ACS Appl. Mater. Interfaces*, 2012, **4** (9), 4506.
31 J. Y. Park, M. J. Baek, E. S. Choi, S. Woo, J. H. Kim, T. J. Kim, J. C. Jung, K. S. Chae, Y. Chang and G. H. Lee, *ACS Nano*, 2009, **3** (11), 3663.
32 H. B. Na, I. C. Song and T. Hyeon, *Adv. Mater.*, 2009, **21**, 2133.
33 R. Di Corato, F. Gazeau, C. Le Visage, D. Fayol, P. Levitz, F. Lux, D. Letourneur, N. Luciani, O. Tillement and C. Wilhelm, *ACS Nano*, 2013, **7** (9), 7500.
34 S. A. Osseni, S. Lechevallier, M. Verelst, P. Perriat, J. Dexpert-Ghys, D. Neumeyer, R. Garcia, F. Mayer, K. Djanashvili, J. A. Peters, E. Magdeleine, H. Gros-Dagnac, P. Celsisf and R. T. Mauricot, *Nanoscale*, 2014, **6**, 555.
35 J. Zhang, Y. Liu and S. Man, *J. Lumin.*, 2006, **117**, 141.
36 M. Mikami and A. Oshiyama, *Phys. Rev. B*, 1999, **60**, 1707.
37 S. Mao,. Liu, M. Gu, D. Mao and C. Chang, *J. Alloys Compd.*, 2008, **465**, 367.
38 B. Lei, Y. Liu, J. Zhang, J. Meng, S. Man and S. Tan, *J. Alloys Compd.,* 2010, **495**, 247.
39 T. H. Shin, Y. Choi, S. Kim and J. Cheon, *Chem. Soc. Rev.*, 2015, **44**, 4501.
40 J. G. Penfield and R. F. Reilly, *Nat. Clin. Pract. Nephrol.*, 2007, **3**, 654.
41 Z. Zhou, L. Wang, X. Chi, J. Bao, L. Yang, W. Zhao, Z. Chen, X. Wang, X. Chen and J. Gao, *ACS Nano*, 2013, **7**, 3287.
42 D. Kryza, J. Taleb, M. Janier, L. Marmuse, I. Miladi, P. Bonazza, C. Louis, P. Perriat, S. Roux, O. Tillement and C. Billotey, *Bioconjugate Chem.*, 2011, **22**, 1145.
43 J. Thirumalai, R. Chandramohan, S. Auluck, T. Mahalingam and S. R. Srikumar, *J. Colloid Interface Sci.*, 2009, **336**, 889.
44 J. Thirumalai, R. Chandramohan, S. Valanarasu, T. A. Vijayan, R. M. Somasundaram, T. Mahalingam and S. R. Srikumar, J. *Mater. Sci.,* 2009, **44**, 3889.
45 G. Blasse, B. C. Grabmaier, Luminescent materials, *Springer Verlag*, 1994.
46 P. A. Rodnyi, *Opt. Spectrosc.*, 2009, **107** (2), 270.
47 P. Dorenbos, *J. of Lum.*, 2007, **122-123**, 315.
48 J. T. Randall and M. H. F. Wilkins, *Proc. R. Soc. A,* 1945, **184**, 366.
49 S. Blahuta, B. Viana, A. Bessiere, E. Mattmann and B. LaCourse, *Opt. Mater.*, 2011, **33** (10), 1514.
50 L. Faucher, A. A. Guay-Begin, J. Lagueux, M. F. Cote, E. Petitclerc and M. A. Fortin, *Contrast Media Mol. Imaging*, 2011, **6**, 209.
51 M. Ahre, L. Selega, F. Soderlind, M. Linares, J. Kauczor, P. Norman, P.-O. Kall, K. Uvdal, *J. Nanopart. Res.*, 2012, **14**, 1006.